Engineering the Interface: Nanodiamond Coating on 3D-Printed Titanium Promotes Mammalian Cell Growth and Inhibits Staphylococcus aureus Colonization

Rifai, Aaqil; Tran, Nhiem; Reineck, Philipp; Elbourne, Aaron; Mayes, Edwin; Sarker, Avik; Dekiwadia, Chaitali

Rifai, A., Tran, N., Reineck, P., Elbourne, A., Mayes, E., Sarker, A., Dekiwadia, C., Ivanova, E., Crawford, R., Ohshima, T., Gibson, B., Greentree, A., Pirogova, E., & Fox, K. (2019). Engineering the Interface: Nanodiamond Coating on 3D-Printed Titanium Promotes Mammalian Cell Growth and Inhibits Staphylococcus aureus Colonization. ACS Applied Materials and Interfaces, 11(27), 24588–24597. https://doi.org/10.1021/acsami.9b07064
Document Version: Accepted Manuscript

Published Version: https://doi.org/10.1021/acsami.9b07064

ACS APPLIED MATERIALS & INTERFACES

Research Article

www.acsami.org

Engineering the Interface: Nanodiamond Coating on 3D-Printed Titanium Promotes Mammalian Cell Growth and Inhibits *Staphylococcus aureus* Colonization

Aaqil Rifai,[*,†] Nhiem Tran,[‡] Philipp Reineck,[§] Aaron Elbourne,[‡] Edwin Mayes,[∥] Avik Sarker,[†] Chaitali Dekiwadia,[∥] Elena P. Ivanova,[‡] Russell J. Crawford,[‡] Takeshi Ohshima,[#] Brant C. Gibson,[§] Andrew D. Greentree,[§] Elena Pirogova,[†] and Kate Fox[*,†,⊥]

[†]School of Engineering, [‡]School of Science, [§]ARC Centre of Excellence for Nanoscale BioPhotonics, School of Science, [∥]RMIT Microscopy and Microanalysis Facility (RMMF), and [⊥]Centre for Additive Manufacturing, RMIT University, Melbourne, VIC 3001, Australia

[#]National Institutes for Quantum and Radiological Science and Technology, Takasaki, Gunma 370-1292, Japan

Supporting Information

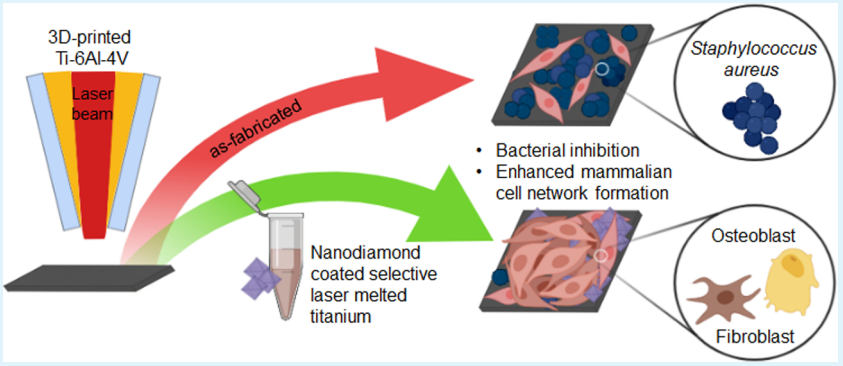

ABSTRACT: Additively manufactured selective laser melted titanium (SLM-Ti) opens the possibility of tailored medical implants for patients. Despite orthopedic implant advancements, significant problems remain with regard to suboptimal osseointegration at the interface between the implant and the surrounding tissue. Here, we show that applying a nanodiamond (ND) coating onto SLM-Ti scaffolds provides an improved surface for mammalian cell growth while inhibiting colonization of *Staphylococcus aureus* bacteria. Owing to the simplicity of our methodology, the approach is suitable for coating SLM-Ti geometries. The ND coating achieved 32 and 29% increases in cell density of human dermal fibroblasts and osteoblasts, respectively, after 3 days of incubation compared with the uncoated SLM-Ti substrate. This increase in cell density complements an 88% reduction in *S. aureus* detected on the ND-coated SLM-Ti substrates. This study paves a way to create facile antifouling SLM-Ti structures for biomedical implants.

KEYWORDS: *nanodiamond, antifouling, 3D printing, biomaterial, implants*

1. INTRODUCTION

Every human is different, and consequently, every manifestation of disease is unique. For this reason, bespoke implants represent an important frontier for improving outcomes in orthopedic surgeries.[1,2] By tailoring implants to the particular physiology of a given patient, it is possible to reduce pain, improve cosmetic outcomes, and ideally reduce the burden of surgery by decreasing the need for secondary replacement procedures being undertaken.[3,4] One key technology for bespoke implants is through the application of computer-aided additive manufacturing methods, which involves the use of three-dimensional (3D) printing technologies.[5] To construct metal implants, selective laser melting (SLM) is one of the preferred technologies of choice. SLM uses powdered metal to bond complex structural forms through a layer-upon-layer process.[3] SLM is a technique that employs high power-density laser to completely melt and fuse metallic powders to create near-net-shaped parts with near-full density (up to 99.9% relative density).[6,7] A variety of metals can be used for SLM,[8] but biomedical implant materials are predominantly limited to stainless steel, cobalt chromium, and titanium. This is mainly due to their biocompatibility and mechanical stability enabling a high strength-to-weight ratio in the implant.[9] SLM can reduce the cost of production and minimize the number of parts required for implant assembly while maintaining the integrity of the implant.

Received: April 23, 2019
Accepted: June 14, 2019
Published: June 14, 2019

DOI: 10.1021/acsami.9b07064
ACS Appl. Mater. Interfaces XXXX, XXX, XXX−XXX

For additively manufactured implants, scaffold designs can be as simple as solid plates or be more complex, such as with lattice structures. Although medical implants are fabricated and designed through careful material selection to integrate well with the underlying hard tissue, device failure remains a risk in both the surgical procedure and through the process of implanting a foreign object into the body. Metallic implant failure is often linked to the formation of implant wear particles[10] and subsequent aseptic loosening[11−14] of the prosthesis. Both situations stimulate macrophages to release cytokines, chemokines, metalloproteinases, and other agents, which then activate osteoclasts, resulting in bone resorption and a reduction in osseointegration.[15,16] More often than not, the implants lack the synergistic effect of promoting both osseointegration and preventing bacterial adhesion. Additionally, biofilm formation may result from bacterial contamination during surgery or due to the attachment of free-floating bacteria on the implant surface. Biofilms can compromise the host immune system in the inflammatory phase, ultimately resulting in implant failure.[17−20] The lack of osseointegration, i.e., the stable anchorage of the implant achieved by direct implant-to-bone contact, also affects the progress of wound healing and reduces the chance of patients recovering at a steady rate.[21] To mitigate these effects, one approach is to explore the application of a secondary implant coating to improve the process of osseointegration, hence preventing the possibility of implant failure.[22−25] Coating surfaces with three-dimensional structures is difficult; the fabrication parameters being used can affect the adherence of the coating, along with its uniformity, roughness, and morphology.[3,22] As a result, nanodiamond (ND) coatings are often realized using a trial-and-error repetitive process to obtain the greatest coverage.

After the initial bacterial attachment to the surface of the implant, the bacteria form a three-dimensional matrix by excreting extracellular polymeric substances (EPSs).[18,26,27] Once the substance is deposited, the bacteria eventually bind to the underlying surface, making it extremely difficult to eradicate. As time passes, the bacteria can reach a critical mass on the implant, forming biofilms. These biofilms are difficult to treat because antibiotics, antiseptics, and host defense mechanisms may not be able to penetrate through the EPS matrix. This is particularly true for orthopedic implants such as intramedullary nails, which are placed in areas with a lack of blood flow. In other circumstances, biofilms can enter a dormant state, becoming difficult to eliminate. If they do not metabolize to maintain activity, antibiotics will not be as effective.[28,29] Hence, it is important for effective sterilization strategies to be used prior to surgery to minimize the chances of biofilm formation from the beginning. Furthermore, implants such as percutaneous implants and internal fixation devices are located among the host body tissue. Therefore, the body undergoes stages of healing and recovery to adapt to the circumstances of having an artificial and foreign material. A synergistic effect, whereby the ND coating prevents bacterial adhesion and still promotes mammalian cell adhesion and proliferation, is a preferable advantage over traditional uncoated metallic implants.

Nanodiamonds (NDs) are rapidly finding biomedical applications due to their reported ability to create a tunable surface through functionalization processes[30,31] and excellent biocompatibility.[32,33] NDs have attracted interest as drug-delivery vehicles,[34] antibacterial agents,[35] biocompatibility enhancers,[36] and promoters of osseointegration.[37,38] As a result, NDs are used in advanced biomedical applications as seeding material coatings,[39−42] thin films, or can be incorporated as a composite material for potential implant imaging applications.[43] In other cases, NDs have been investigated and reviewed as potential antibacterial surfaces.[44] Numerous studies have looked at the differential adhesion of bacterial species to titanium substrata,[45−49] some of which have often revealed contradictory results. The control of biofouling via roughness and surface architecture mainly mediates the focus of these reports.

In this study, we have demonstrated that a coating of NDs can improve the interfacial properties of three-dimensional selective laser melted titanium (SLM-Ti) plates (ND-SLM-Ti). We evaluated coating methodologies in suspensions with different ND concentrations and evaluated the effect of surface coverage on the properties of the substrata, showing that the wettability of the SLM-Ti varied from being hydrophobic to hydrophilic upon the addition of NDs. The resultant ND-SLM-Ti substratum was shown to promote the growth of human dermal fibroblast (HDF) and osteoblast (OB) cells while inhibiting the adhesion of *Staphylococcus aureus*. The ND-coated SLM-Ti substrata synergistically promote osseointegration and inhibit bacterial adhesion. Our findings suggest that NDs can be readily coated onto SLM-Ti substrata as a facile approach to improve the biocompatibility of surgical implants.

2. EXPERIMENTAL SECTION

2.1. Synthesis of ND-Coated SLM-Ti Substrata. *2.1.1. Sample Preparation.* Additively manufactured SLM-Ti substrata (10 × 10 × 0.5 mm^3) were fabricated using the method detailed by Xu et al.[50] Standard cleaning of SLM-Ti substrata was performed using a process of sequential sonication in acetone, methanol, and isopropanol followed by drying under a steady flow of nitrogen gas.

2.1.2. Diamond Coating. SLM-Ti substrata were seeded with as-received 120 nm ND powder (Nabond Technologies, China). The ND powder was suspended in a water solvent at a concentration of 7.5% w/v. This stock suspension was further diluted to achieve suspensions of 0.75 and 0.075% w/v concentrations. The SLM-Ti substrata were coated using a dip-coating technique, where substrata were placed into different concentrations of ND suspensions using the method described elsewhere or according to previously published protocols.[51−53] A single dip in each concentration of the ND suspension was performed, coating a single side of the substratum. The solvent was then allowed to dry. An ASTM D 3359[54] adhesion tape test confirmed the adhesion strength to be 4 out of 5. The tape shows less than 5% detachment of ND particles from the underlying SLM-Ti substrate. The adhesion test is repeated three times to ensure that results are satisfactory.

To visualize whether the cells and bacteria colocalize with the NDs, 120 nm NDs were irradiated at 2 MeV (IrrND) (in line with that reported by Fox et al.[43]). The IrrND suspension with the concentrations of 0.075, 0.75, and 7.5% w/v was deposited onto the SLM-Ti substrata.

2.2. Material Characterization. Scanning electron microscope (SEM) images were obtained using xT Nova Nanolab 200 and JEOL JSM-5910 scanning electron microscopes, using an acceleration voltage of 30 kV for faces and 15 kV for edge imaging.

X-ray photoelectron spectroscopy (XPS) (Thermo Fisher K-Alpha) was used to obtain the chemical composition of the ND-coated samples with the Al Kα radiation source at a power of 300 W. The spot size of analysis was 400 μm. Sample scanning was performed using the flood gun function to compensate for charging and the auto height function for the determination of the optimal distance for the X-ray beam and the sample. The elements detected in the surface layers (analysis depth 2−5 nm) were observed from the survey spectrum (pass energy 200 eV) over a range of 0−1100 eV (step size

DOI: 10.1021/acsami.9b07064
ACS Appl. Mater. Interfaces XXXX, XXX, XXX−XXX

1 eV, dwell time 50 ms). The XPS binding energy (BE) values obtained from the high-resolution scans of elemental signals (pass energy 50 eV) were not charge-corrected with respect to that of adventitious carbon at 284.8 eV due to the scanning being undertaken using the flood gun. In particular, high-resolution XPS spectra were collected for the critical elements carbon, oxygen, and titanium, as identified from the survey spectra. High-resolution scanning was undertaken with a step size of 0.1 eV and a dwell time of 50 ms.

A PerkinElmer 2000 infrared spectrometer was used to analyze the chemical bonds in the ND and SLM-Ti samples. The functional group vibrations of the SLM-Ti and ND were analyzed using Fourier-transform infrared spectroscopy (FTIR) spectra. The ND was analyzed using FTIR using a potassium bromide pellet. The FTIR spectra were obtained for 32 scans at a resolution of 4 cm^{-1} over a range of 0−4000 cm^{-1}. Background spectra were obtained in the chamber for a sample holder without samples before the actual analysis. The inclination angle of the measured surface was then adjusted for high energy before scanning. Inbuilt software was then used for processing the acquired spectra. At least three measurements were carried out for each sample.

An XP-2 Stylus Profiler (Ambios Technology, Inc.) was used to determine the surface roughness of the samples. The surface roughness (R_a > 1 μm) was measured at a force of 0.1 mg and a scan rate of 0.01 mm/s over an area of 0.5 mm. The R_a value was obtained by averaging the values obtained across each sample. Gwyddion software was used to determine the surface roughness parameters.

The surface wettability of the samples was characterized using contact angle goniometry. Static water contact angle measurements were performed using a Drop Shape Analyzer (Kruss, Hamburg, Germany) at room temperature. Images were acquired using inbuilt software. The contact angles reported in this work were the average of those taken from five distinct places on the surface of each sample.

2.3. Mammalian Cell Assessment of ND-Coated SLM-Ti Substrata. The viability and proliferation of human dermal fibroblast (HDF) cells (ATCC PCS-201-010, ATCC, Manassas) on the surface of the ND-SLM-Ti substrata were determined using fluorescence microscopy and 3-(4,5-dimethylthiazol-2-yl)-2,5-diphenyltetrazolium bromide (MTS) assay (CellTiter 96 AQueous One Solution (Promega) according to the manufacturer's suggested protocol). Uncoated SLM-Ti samples and tissue culture plastic (TCP) were used as controls. HDF cells were selected as they have been commonly reported to measure cytotoxicity and biocompatibility for materials used in biomedical applications in addition to examining potential applicability toward percutaneous implants.[55] Prior to cell seeding, all of the samples were autoclaved to ensure that surfaces were sterile. For fluorescence microscopy, the samples were placed into a 24-well plate and seeded with HDF cells in Dulbecco's modified Eagle's medium (DMEM) (supplemented with 10% fetal bovine serum (FBS) and 1% penicillin/streptomycin (P/S)) (all obtained from Gibco, Life Technologies) at a density of 4×10^4 cells/cm^2. The well plate was incubated for 1, 3, and 5 days at a temperature of 37 °C under 5% CO_2. After incubation, cells were rinsed with phosphate-buffered saline (PBS). Then, paraformaldehyde was applied for 30 min to fix the cells. The cells were permeabilized and blocked with 0.3% Triton X-100 and 1% bovine serum albumin (BSA), respectively, and were washed three times with PBS. The actin filaments were then stained with Alexa Fluor 594 Phalloidin (1:40 dilution, Thermo Fisher Scientific, Scoresby, VIC, Australia) and incubated for 2 h at room temperature. Then, 1 μL of Hoechst 33258 (Thermo Fisher Scientific) was added to the cells for 5 min to stain the nucleus. The samples were washed with PBS and stored with 1 mL of PBS at 4 °C for fluorescent microscopy imaging (Olympus confocal microscope FV1200). For an additional assessment of colocalization between the HDF and NDs, the HDFs were grown on a set of SLM-Ti substrata coated with IrrND. The nucleus and the actin filaments were captured using a 4′,6-diamidino-2-phenylindole (DAPI) filter (350/470 nm) and a tetramethylrhodamine filter (561/600 nm), respectively. Higher-resolution fluorescent images were also captured by using a Nikon confocal laser scanning microscope (CLSM) with an N-STORM Super-Resolution system to assess the extent of cell growth across the surface. In these images, IrrND on the substrata were captured using a Cy5 filter with Ex/Em wavelengths of 559 and 700 nm. To show a clear distinction between the actin filaments and IrrNDs, the high-resolution images of actin filaments and IrrNDs were false colored in green and red, respectively.

For MTS cell viability assays, 4×10^4 cells/cm^2 were seeded on SLM-Ti and ND-SLM-Ti samples in a 24-well plate. The plate was incubated at 37 °C in a CO_2 incubator for 1, 3, and 5 days. After this time, 200 μL of CellTiter 96 AQueous One Solution (Promega, Madison, WI) was added to the wells according to the manufacturer's recommendation. The cells were incubated at 37 °C for an additional 3 h. A 100 μL aliquot of cell solution was then transferred to a 96-well plate, and absorbance at 490 nm was recorded using a plate reader (SpectraMax Paradigm, Molecular Devices, Sunnyvale). The resulting optical density (OD) could be directly correlated to the viable cell numbers. Each experiment was performed in triplicates and was repeated three times.

The cell densities of rat calvariae primary osteoblasts (OBs) (R-Ost-583, Lonza, Walkersville) grown on the surface of the ND-SLM-Ti substrata were determined using fluorescence microscopy and an MTS assay (CellTiter 96 AQueous One Solution (Promega) according to the manufacturer's suggested protocol). Uncoated SLM-Ti samples and tissue culture plastic (TCP) were used as controls. OB cells were selected as they are bone-forming cells. These cells are particularly important to determine the osseointegration with the samples for orthopedic applications.[36,56] Prior to cell seeding, all of the samples were autoclaved to ensure that surfaces were sterile. For fluorescence microscopy, the samples were placed into a 24-well plate and seeded with OB cells in DMEM with 4.5 g/L glucose (Lonza No. 12-604F) supplemented with the rat MSCGM SingleQuots kit (Lonza No. 00192820). The rat MSCGMTM SingleQuots kit contains 50 mL of FBS (10% final concentration in media), L-glutamine, and GA-1000. The rMSC osteogenic SingleQuots kit contains 20 mL of FBS (10% final concentration in media), L-glutamine, GA-1000, ascorbate, dexamethasone, and β-glycerophosphate (all obtained from Lonza) at a density of 5000 cells/cm^2. The well plate was incubated for 3 days at a temperature of 37 °C under 5% CO_2. After incubation, cells were rinsed with phosphate-buffered saline (PBS). Then, paraformaldehyde was applied for 30 min to fix the cells. The cells were permeabilized and blocked with 0.3% Triton X-100 and 1% BSA, respectively, and were washed three times with PBS. The actin filaments were then stained with Alexa Fluor 594 Phalloidin (1:40 dilution, Thermo Fisher Scientific, Scoresby, VIC, Australia) and incubated for 2 h at room temperature. Then, 1 μL of 300 nM 4′,6-diamidino-2-phenylindole (DAPI, dihydrochloride) (Thermo Fisher Scientific) was added to the cells for 5 min to stain the nucleus. The samples were washed with PBS and stored with 1 mL of PBS at 4 °C for fluorescent microscopy imaging (Olympus confocal microscope FV1200).

For MTS cell viability assays, 5000 cells/cm^2 were seeded on SLM-Ti and ND-SLM-Ti samples in a 24-well plate. The plate was incubated at 37 °C in a CO_2 incubator for 3 days. After this time, 200 μL of CellTiter 96 AQueous One Solution (Promega, Madison, WI) solution was added to the wells according to the manufacturer's recommendation. The cells were incubated at 37 °C for an additional 3 h. A 100 μL aliquot of cell solution was then transferred to a 96-well plate, and absorbance at 490 nm was recorded using a plate reader (SpectramMax Paradigm, Molecular Devices, Sunnyvale). The resulting optical density (OD) could be directly correlated to the viable cell numbers. Each experiment was performed in triplicates and was repeated three times.

2.4. Antibacterial Property of ND-Coated SLM-Ti Substrata. The *S. aureus* CIP 65.8^T was obtained from the Bacterial Culture Collection of Institute Pasteur, France. Bacterial stocks were prepared in 20% glycerol nutrient broth (NB, Oxoid, Thermo Fisher Scientific, Scoresby, VIC, Australia) and stored at −80 °C until needed. Prior to the experiment, the stock was refreshed upon nutrient agar (Oxoid) for 24 h at 37 °C. *S. aureus* suspensions were prepared by suspending one loopful of bacteria into 5 mL of NB. The suspensions were then

DOI: 10.1021/acsami.9b07064
ACS Appl. Mater. Interfaces XXXX, XXX, XXX−XXX

further diluted using the nutrient broth to obtain an optical density OD_{600} = 0.1. The SLM-Ti and ND-SLM-Ti samples were sterilized with repeated washes of ethanol, rinsed with Milli-Q water, and dried under a gentle N_2 flow. The sterilized surfaces were then incubated in 1 mL of bacterial suspension in a sterilized 12-well plate (In Vitro Technologies, Noble Park, VIC, Australia) for a duration of 18 h at 25 °C.

Following the incubation period, CLSM was utilized to assess the surface adhesion of live and dead bacteria. Prior to CLSM imaging, samples were removed from the bacterial suspensions and washed gently twice with Milli-Q water for 3 s. This process removes unattached bacteria from the surface, allowing all imaging experiments to be performed under similar conditions. Surface bacteria were then stained for 30 min in the dark using a LIVE/DEAD BacLight Bacterial Viability Kit, L7012 (Molecular Probes, Life Technologies), according to the manufacturer's protocol. SYTO9 permeates both intact and damaged membranes of the cells and fluoresces green when bound to nucleic acids and excited by laser light at 485 nm wavelength; however, propidium iodide (PI) only enters bacteria with significant membrane damage (nonviable cells) and binds with higher affinity to the intracellular nucleic acids than SYTO9. The proportion of each type of bacteria was determined by pixel counting at their respective fluorescence emission wavelengths. CLSM images were obtained using an FV1000 Spectroscopic Confocal System (Olympus, Tokyo, Japan). Images were taken for five different fields of view to obtain the representative data for the entire surface using the *z*-stack function. The *z*-stack function is critical to obtain the full depth of view from the upper to lower limits of the substrata. After image acquisition, imaging software Fluoview FV 4.2 was utilized to assess the CLSM images on a frame-by-frame basis, which allows the total surface-cell count to be calculated. The number of surface-adsorbed cells was quantified using Cell-C (https://sites.google.com/site/cellcsoftware/), which provides a meaningful assessment of the antifouling activity of the surface. Importantly, discrepancies in the viability assessment were avoided by ensuring that no green (485 nm) and red (543 nm) fluorescence overlap was observed during image assessment. This means that live and dead cell differentiation was adequately achieved, providing meaningful assessment of the surface antibacterial activity.

In addition to CLSM, SEM micrographs of corresponding sample surfaces were obtained using the FEI Scios Dualbeam scanning electron microscope, using an acceleration voltage of 30 kV. These SEM micrographs confirm the trends observed using CLSM.

3. RESULTS AND DISCUSSION

3.1. ND-Coated SLM-Ti Surface Characterization.

Figure 1a shows an SEM micrograph of the SLM-Ti surface topography prior to ND coating. The micrograph reveals numerous partially melted titanium particles, which have been produced during the manufacturing of the SLM-Ti sample. As reported previously,[57] these partially melted titanium particles can vary between 20 and 50 μm in height,[22,57] which is large, compared with the nominal ND size of 120 nm. Similarly, Figure 1b shows the SEM micrograph of the ND-SLM-Ti. The high-magnification inset in Figure 1b reveals that ND adhered to the surface of the SLM-Ti substratum. The high-resolution carbon XPS spectra show the surface groups on the ND-SLM-Ti substratum in comparison with the bare SLM-Ti. The XPS spectra reveal distinct spectral peaks at binding energies of 284 and 284.8 eV in the high-resolution C 1s spectrum, which can be assigned to the sp^2 and the sp^3 C−C bond, respectively, of the ND. The sp^2 and sp^3 hybridizations of the nanodiamond reportedly promote chemical and biological integration at the tissue−implant interface.[30,43] Peaks detected at 286 and 288.4 eV could be attributed to C−O and O−C═O, respectively.[58,59] These functional groups originate as a consequence of the manufacturing process of the as-received NDs.

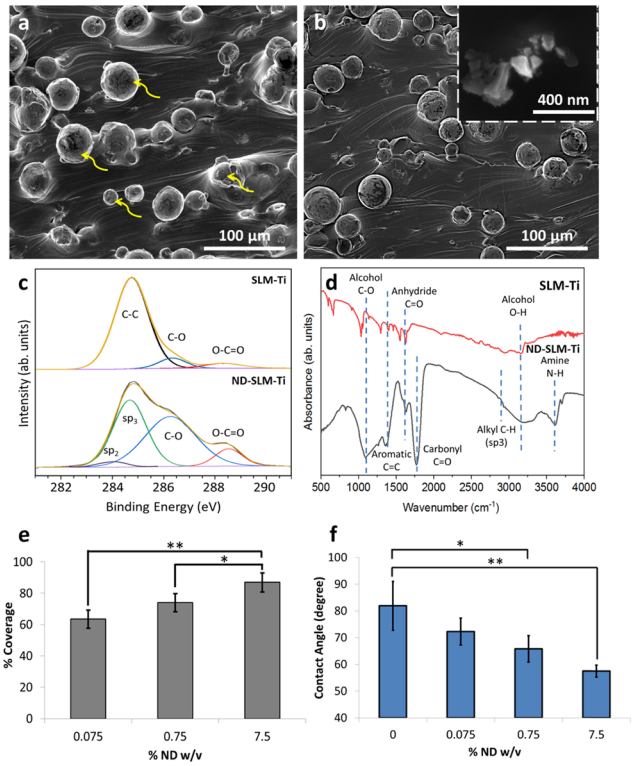

Figure 1. Surface characterization of nanodiamond (ND)-coated selective laser melted titanium (SLM-Ti) substrata (ND-SLM-Ti). (a) SEM image of the uncoated SLM-Ti substrata showing a large volume of partially melted particles (indicated by the yellow arrows). (b) SEM image of the ND-SLM-Ti substrata showing an inset of the ND attached to the surface of the SLM-Ti. (c) C 1s (carbon) high-resolution XPS spectra of uncoated SLM-Ti (top) showing peaks fitted for C−C, C−O, and O−C═O bonds. In contrast, as-received ND (bottom) shows peaks fitted for sp^2, sp^3, C−O, and O−C═O bonds. (d) FTIR spectra of uncoated SLM-Ti and as-received ND obtained using a potassium bromide pellet, detailing surface functional groups. Relative to SLM-Ti, ND adsorption regions indicate bonds of C−O, C═C, C═O, sp^3, O−H, and N−H. (e) Surface coverage of ND over a 1 × 1 cm^2 dip-coated substratum in relation to the concentration of ND suspensions. Data = mean ± standard deviation. Coverage: * $p < 0.05$ and ** $p < 0.005$. (f) Water contact angle of the ND-coated SLM-Ti substrata. Data = mean ± standard deviation. Contact angle: * $p < 0.01$ and ** $p \leq 0.002$.

The FTIR spectra of ND-SLM-Ti compared with the bare SLM-Ti are presented in Figure 1d. The FTIR absorption bands from the ND revealed an anhydride bond between 1750 and 1850 cm^{-1} (C═O). Other oxygen-containing functional groups were found to be present, such as the hydroxyl group (O−H) between 3200 and 3600 cm^{-1} and (C−O) between 1050 and 1150 cm^{-1}. Amines (N−H) also exist between 3300 and 3600 cm^{-1}, with an alkyl group (C−H) derived from sp^3 between 2800 and 3000 cm^{-1}, carbonyl stretch (C═O) at 1840 cm^{-1}, and an aromatic group (C═C) found between 1400 and 1600 cm^{-1}. These bonds are expected to be dangling bonds on the surface of the ND following exposure to air at room temperature.[31] Similar observations of such ND surface chemistry were observed using XPS and FTIR spectroscopy by Zhao et al.[60]

The surface coverage of ND dispersed by dip-coating over a 1 × 1 cm^2 SLM-Ti surface is shown in a column graph in Figure 1e, where the quantification of the coverage area was obtained using ImageJ.[61] As expected, the higher the

DOI: 10.1021/acsami.9b07064
ACS Appl. Mater. Interfaces XXXX, XXX, XXX−XXX

suspension concentration of ND, the higher the coverage of the SLM-Ti surface with ND. At a concentration of 7.5% w/v ND, the coverage was determined to be on average 87% compared with coverages of 65 and 76% for concentrations of 0.075% w/v ND and 0.75% w/v ND, respectively. Although the biological effects that we report below are all a function of the ND coverage (rather than the concentration of the suspension that generated that coverage), the samples will be labeled according to the concentration of the ND suspension used to prepare the samples. An ASTM D 3359[54] adhesion tape test was performed, similar to our previous study examining polycrystalline diamond (PCD) coatings,[22] whereby the adhesion strength was deemed to be 4 out of 5. The tape shows less than 5% detachment of ND particles from the underlying SLM-Ti substrate. The adhesion test is repeated three times to ensure that results are satisfactory.

The water contact angle measured at the ND interface shows an increase in the hydrophilicity (i.e., decrease of water contact angle) of the substratum with increasing ND coverage, as shown in Figure 1f. As the concentration of NDs increases, the contact angle decreases, highlighting that the NDs can be used to tune the wettability of the substratum surface. The water contact angle of the uncoated SLM-Ti substratum is 81.9 ± 9.1°, which is consistent with our previously reported results.[22] Using the low ND concentration suspension (0.075% w/v) had a negligible effect on the wettability of the substratum, with a measured contact angle of 72°. As NDs were added in larger concentrations (0.75 and 7.5% w/v, respectively), the contact angle continued to decrease such that the surface became increasingly hydrophilic ($p \leq 0.002$). As the surface became increasingly hydrophilic, the interface became more attractive for cell adhesion and subsequent proliferation.[62,63] It is likely that the O−H bonds present on the surface of the NDs (Figure 1d) were responsible for the increased hydrophilicity at the interface.[31,64,65]

3.2. Influence of ND Coating on Mammalian Cell Growth. Figure 2a−d shows confocal fluorescence images of human dermal fibroblasts (HDFs) grown on SLM-Ti and SLM-Ti coated using 0.075, 0.75, and 7.5% w/v aqueous ND suspensions following 3 days of growth. A comparison of the confocal images by cell count (data not shown) and by further analysis of the MTS assay reveals that increasing the ND suspension concentration increased the density of the HDF cells (Figure 2b−d). The confocal micrographs show that the HDFs appeared to stretch, forming cojoining networks, showing signs of preferable adhesion and proliferation to the ND-SLM-Ti substratum to that observed on the SLM-Ti substratum. More prominently, at the highest ND concentration, the growth of a multilayered cellular network was apparent (Figure 2d and Video S1), which suggests that NDs may improve cellular integration on the implant and therefore adhesion.

The cell viability was assessed after 1, 3, and 5 days of HDF growth on all substrata using the MTS assay. From Figure 2e, it is apparent that HDF density rises with increasing ND concentration on the substrata. After 1 day of incubation, the cell density of the SLM-Ti increased by 33% with the addition of 7.5% w/v ND, which was from 78 000 cell/cm^2 (SLM-Ti) to 117 000 cell/cm^2 (7.5% w/v ND). At the final incubation period of 5 days, there was a 20% increase in HDF density for SLM-Ti, compared with a 10% increase in HDF density for the ND-SLM-Ti substratum coated with the highest ND concentration of 7.5% w/v ND. The HDF density after 5 days shows that 96 200 cell/cm^2 were attached to the SLM-Ti substratum compared with the HDF density of 127 400 cell/cm^2 for the 7.5% w/v ND. This is a 24% increase in HDF density with the ND coating. Individual ND particles are small in diameter compared with the larger partially melted particles on the titanium surface. The increase in HDF adhesion in response to the ND concentration reported herein is consistent with our recent findings of favorable Chinese Hamster Ovarian cell adhesion onto polycrystalline diamond (PCD)-coated SLM-Ti surfaces.[22]

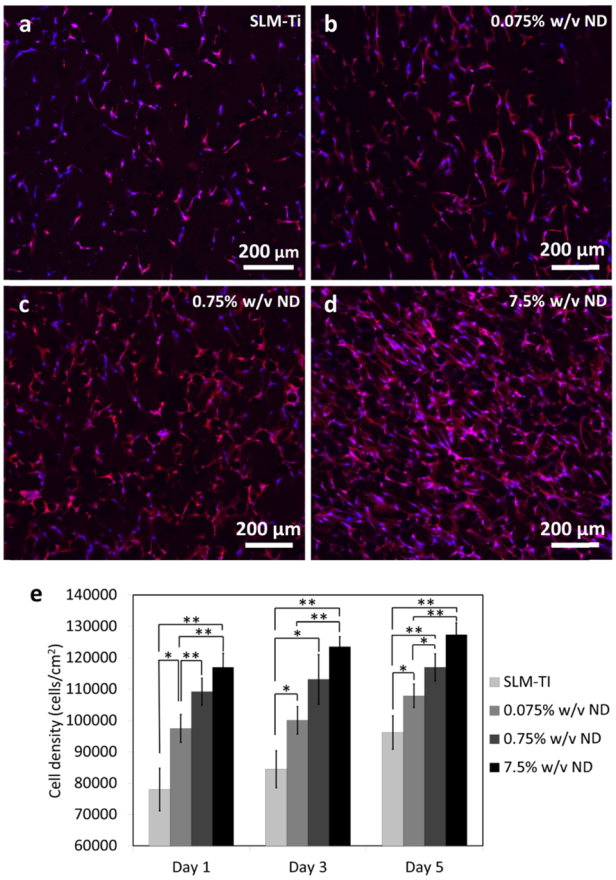

Figure 2. Influence of nanodiamond (ND) coverage on selective laser melted titanium (ND-SLM-Ti) on human dermal fibroblasts (HDFs). Fluorescence images showing ND-SLM-Ti substrata with progressive HDF growth on 0.075, 0.75, and 7.5% w/v ND suspensions in comparison to the bare SLM-Ti after a 3 day incubation period. (a) Uncoated SLM-Ti control. (b) 0.075% w/v ND, (c) 0.75% w/v ND, and (d) 7.5% w/v ND. Staining for the nuclei is Hoechst (blue) and for actin filaments it is Alexa Flour 594. (e) HDF cell density after 1, 3, and 5 days of culture on various ND-SLM-Ti samples as measured by an MTS assay. Data = mean ± standard deviation. * $p \leq 0.05$ and ** $p \leq 0.01$.

To investigate the influence of the ND coatings on the HDF cell morphology and cytoskeletal structure, high-resolution fluorescent confocal images of the cells were obtained (Figure 3a−d). Overall, the cells were observed to grow well on all of the substrata, including the uncoated SLM-Ti substratum. These cells appeared to elongate distinctively around the partially melted particles present on the surface compared with that observed on the planar regions of the surface. This elongation around the partially melted particles supports the recent findings by Sarker et al.[57] Moreover, the cells were also found to spread to equal extents with or without NDs (Figure

DOI: 10.1021/acsami.9b07064
ACS Appl. Mater. Interfaces XXXX, XXX, XXX−XXX

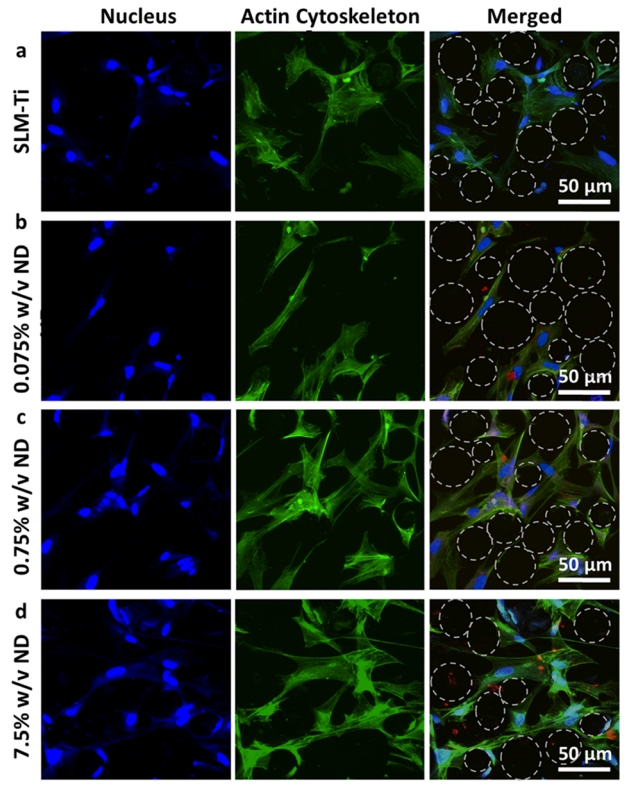

Figure 3. Morphology of human dermal fibroblast (HDF) cells growing on nanodiamond-coated selective laser melted titanium (SLM-Ti) substrata after 3 days of incubation on (a) uncoated SLM-Ti control. (b) Low concentration of ND (0.075% w/v). (c) Medium concentration of ND (0.75% w/v). (d) High concentration of ND (7.5% w/v). Staining for the nuclei is Hoechst (blue) and for actin filaments it is Alexa Flour 594 Phalloidin (false-colored green). The IrrND is shown in red. The dotted gray circles represent the partial SLM-Ti particles on the substrata, which are out of the cell focal plane.

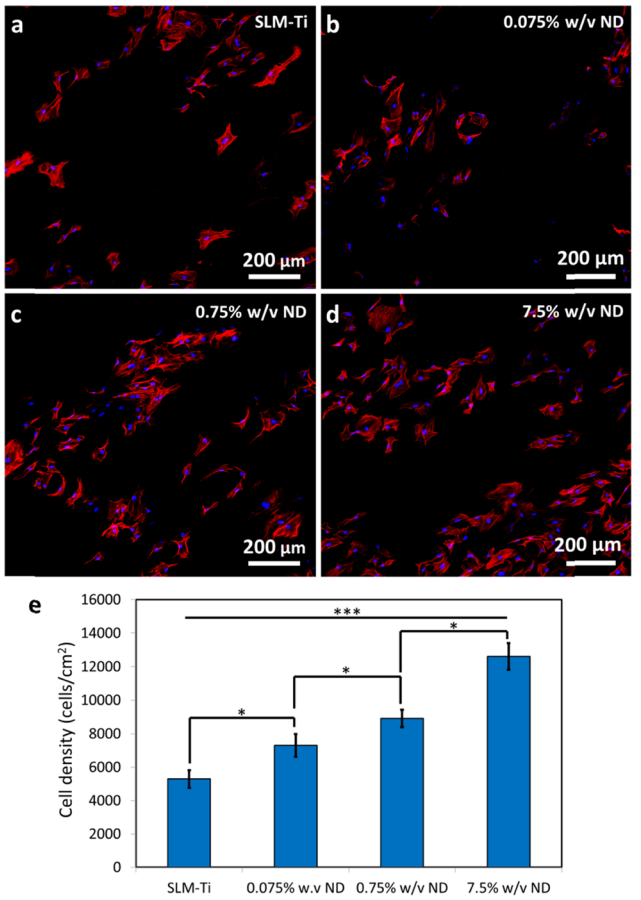

Figure 4. Influence of nanodiamond (ND) coverage on selective laser melted titanium (ND-SLM-Ti) on rat primary osteoblasts (OBs). Confocal fluorescence images showing ND-SLM-Ti substrata with progressive OB growth on 0.075, 0.75, and 7.5% w/v ND suspensions in comparison to the bare SLM-Ti after a 3 day incubation period. (a) Uncoated SLM-Ti control. (b) 0.075% w/v ND, (c) 0.75% w/v ND, and (d) 7.5% w/v ND. Staining for the nuclei is DAPI (blue) and for actin filaments it is Alexa Fluor 594 (red). (e) OB cell density after 3 days of culture on various ND-SLM-Ti samples as measured by an MTS assay. Data = mean ± standard deviation. * $p \leq 0.05$ and *** $p \leq 0.001$.

3). Overall, the biocompatibility tests performed in this study support previous findings, which suggests that NDs are less cytotoxic than many other known carbon nanomaterials.[66,67] For example, Zhang et al.[36] demonstrated that osteoblasts proliferated similarly on scaffolds made of poly(L-lactic acid) containing 0−10 wt % of octadecylamine-functionalized ND during a 6 day cell culture period.[36] Similarly, Mansoorianfar et al.[37] found that alginate-bioactive glass coatings containing ND showed no cytotoxicity to human osteoblasts (MG-63) and mouse fibroblasts (L-929).[37] NDs are widely classified as noncytotoxic[36,37] for applications in drug delivery,[34] sutures,[43] antibacterial agents,[35] and biosensing.[68] Interestingly, in our current study, ND-SLM-Ti surfaces are not only biocompatible but also stimulate a faster HDF growth compared with that observed on the uncoated substrata in a concentration-dependent manner. While the precise mechanism underlying cell growth enhancement needs further study, it is likely that both surface wettability and the micro-/nanosurface roughness contribute toward the physiochemical attraction of the resulting cellular networks on the ND-SLM-Ti substrata.

To complement the viability of HDF, we assessed the biocompatibility of primary osteoblasts (OBs) on ND-SLM-Ti. The confocal results show increasing cell density in a concentration-dependent manner (Figure 4). The cell densities of OB on the SLM-Ti (Figure 4a), 0.075% w/v ND (Figure 4b), 0.75% w/v ND (Figure 4c), and 7.5% w/v ND (Figure 4d) confirm favorable adhesion and proliferation to the samples with an increasing content of ND.

The MTS assay (Figure 4e) showed the cell viability of the OB. The highest increase in cell density was observed to be 58% between SLM-Ti and 7.5% w/v ND. We find that increasing surface coverage of ND leads to increased osteoblast attachment, although this increase was not linear in the concentration of the ND used for coating. We compared four surfaces, as-printed SLM-Ti (control), SLM-Ti-coated 0.075% w/v ND, SLM-Ti-coated 0.75% w/v ND, and SLM-Ti-coated 7.5% w/v ND. After 3 days, the cell attachment was found to be 5300 cells/cm^2 (as-printed SLM-Ti), 7300 cells/cm^2 (SLM-Ti-coated 0.075%), 8900 cells/cm^2 (SLM-Ti-coated 0.75%), and 12 600 cells/cm^2 (SLM-Ti-coated 7.5%). Our results are in broad agreement with those of Yang et al.[56] showing preferential attachment of osteoblasts on the ND-coated substrata. Nevertheless, we are not yet able to show an "optimal" ND coverage for osteoblast growth.

3.3. *S. aureus* Adhesion and Growth on ND-Coated SLM-Ti Substrata. In addition to improving osseointegration,

DOI: 10.1021/acsami.9b07064
ACS Appl. Mater. Interfaces XXXX, XXX, XXX−XXX

an ideal orthopedic implant should prevent the growth of pathogens. In this study, *S. aureus* were selected because they are one of the most common pathogens that are associated with infections in orthopedics and percutaneous implants. *S. aureus* were allowed to attach and grow on uncoated and ND-coated SLM-Ti substrata for a period of 18 h (Figure 5). This

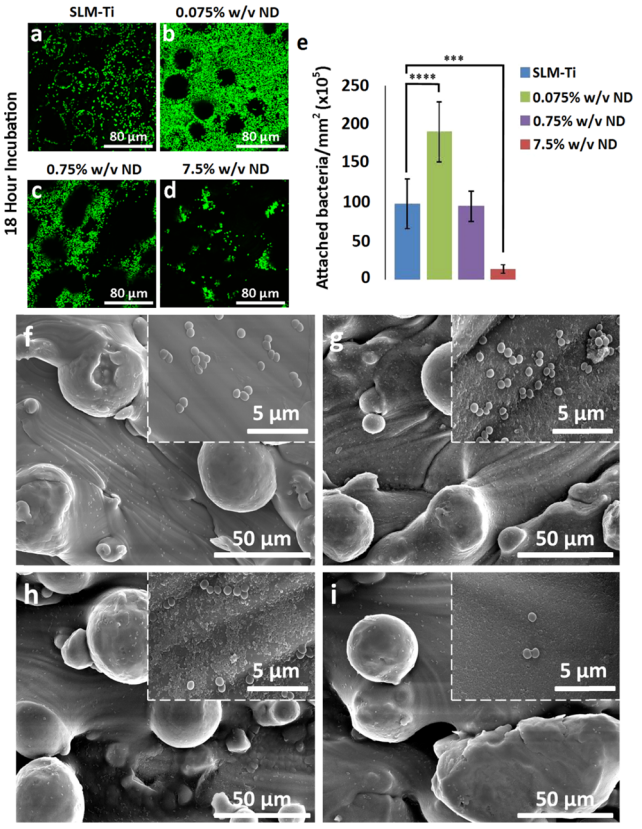

Figure 5. *S. aureus* adhesion and growth on nanodiamond (ND)-coated selective laser melted titanium (ND) substrata (ND-SLM-Ti). *S. aureus* growth on (a) uncoated SLM-Ti substrata, (b) 0.075% w/v ND-SLM-Ti, (c) 0.75% w/v ND-SLM-Ti, and (d) 7.5% w/v ND-SLM-Ti substrata after 18 h of incubation. Live *S. aureus* were stained green. (e) Bar graph represents *S. aureus* density quantified from fluorescent images. Data = mean ± standard deviation, $n = 3$. $p < 0.01$. The bacterial density is shown by the average cell number per mm^2 on each scaffold. The SEM images represent *S. aureus* adhesion on (f) uncoated SLM-Ti substrata, (g) 0.075% w/v ND-SLM-Ti, (h) 0.75% w/v ND-SLM-Ti, and (i) 7.5% w/v ND-SLM-Ti substrata after 18 h of incubation. The SEM micrographs show an overview at low magnification (1000×) and high magnification (30 000×) in the inset.

incubation period has been shown to be sufficient for *S. aureus* to form a monolayer of cells on a substratum.[48,69] Figure 5a shows the bacterial adhesion on the control substratum, SLM-Ti. At the lowest tested ND concentration of 0.075% w/v (Figure 5b), there were more *S. aureus* adhered to the substratum compared with the uncoated SLM-Ti. However, after increasing the ND concentration to 0.75% w/v, the *S. aureus* density reduced by 50% compared with that observed on the substratum prepared using a 0.075% w/v ND suspension (Figure 5c). Finally, the substratum prepared using the highest concentration of ND (7.5% w/v) showed an 88% reduction in *S. aureus* adherence compared with that observed on the uncoated SLM-Ti substrata and a 16-fold decrease compared with the substratum suspended using 0.075% w/v ND (Figure 5d). The live bacterial count shows qualitative information regarding the number of adhered bacteria to the surface (Figure 5e). To further validate the adhesion of *S. aureus* on the substrata, we examined all samples using SEM (Figure 5f–i). The SEM micrographs confirm that the bacterial adhesion was similar to that observed using confocal microscopy.

A direct comparison between the addition of ND coatings to prevent fouling and the extent of mammalian cell growth is difficult. NDs have been shown to inhibit both Gram-positive and Gram-negative bacterial growth.[35,70−72] Most of these studies showed that the adhesion of bacteria is mainly related to the physiochemical properties of the substratum and whether the bacterial cell's surface is hydrophilic or hydrophobic.[27] For ND-coated surfaces, it is likely that, in addition to surface roughness and wettability, the ND surface chemistry, particle size, and concentration all influence the ability of the substratum to prevent or reduce the extent of bacterial adhesion. Several studies such as by Wehling et al.[35] discuss the mechanism of ND showing antibacterial properties. They showed that partially oxidized and negatively charged NDs reduced the bacterial viability of both Gram-negative *Escherichia coli* and Gram-positive *Bacillus subtilis*, whereas positively charged NDs did not adversely affect their viability. The role of functional surface groups is extensively discussed as the primary factor for bacterial inhibition and death. The surface functionalization of NDs with specific groups such as −COOH, −OH, and especially the amine bond $-NH_2$ has been shown to impart greater antibacterial properties to substrata than obtained using nonfunctionalized ND. We use a similar type of ND to that of "raw and no ultrasonication" ND as mentioned in the study of Wehling et al.[35] Therefore, increasing the concentration of ND may be responsible for exhibiting a larger dose of oxidization in addition to the functional groups that inhibit bacterial adhesion or metabolic activity. However, it is unexpected that the lowest concentration of ND (0.075% w/v) has more bacterial adhesion than on uncoated SLM-Ti. This occurrence could have more than one competing factor associated with it. Possible adhesive responses of bacteria could have likely been provoked by either the wettability or nanoroughness of ND.[49,71,73] Braem et al.[49] discuss the wettability and roughness of titanium substrata as the major determinants toward bacterial adhesion and biofilm formation. The micron-range surface roughness and a hydrophobic surface promoted *S. aureus* adhesion. Modes of chemical etching and polishing can be used to alter the wettability and surface roughness. Furthermore, the wettability of *S. aureus* is defined as hydrophobic at the surface of the cell membrane. Therefore, *S. aureus* tend to be attracted toward hydrophobic surfaces.[74] In comparison, the NDs used in our study create substratum surfaces that are hydrophilic. However, the wettability parameters do not contribute toward the increase in bacterial adhesion on the 0.075% w/v ND substrata.

Likewise, rough surface topographies, either random or aligned orientation on the substratum, may increase bacterial attachment. The metabolic activity of *S. aureus* increases after attachment to the surface, leading to biofilm formation.[35,48,74] In comparison to Braem et al.,[49] the effect of the surface roughness in the micron range may not be considered to be the key influencer in bacterial adhesion and proliferation in our study due to the magnitude of the PMPs on the SLM-Ti. In fact, the measured average roughness values 8.67 μm for SLM-

DOI: 10.1021/acsami.9b07064
ACS Appl. Mater. Interfaces XXXX, XXX, XXX−XXX

Ti, 10.1 μm for 0.075% w/v ND, 11.8 μm for 0.75% w/v ND, and 7.79 μm for 7.5% w/v ND (results not shown) do not have any correlation with the concentration of the ND suspended on the SLM-Ti surface. In another instance, Beranová et al.[72] added as-fabricated ND particles using Gram-negative *Escherichia coli* to limit the functionality of the bacteria to multiply and form colonies in a concentration-dependent manner. The NDs with concentrations of 5 μg/mL reduced the bacterial viability to 25%, whereas concentrations above 50 μg/mL completely eradicated the bacteria.[72]

Finally, the major cause preventing bacterial adhesion is due to the chemical composition of NDs. The oxygen and amine groups that are naturally present in the NDs inhibit bacterial adhesion at the highest concentration (7.5% w/v ND). Although the microroughness measurements may ignore the presence of ND due to the PMPs on the surface, more number of *S. aureus* could be adhered due to the nanoscale roughness of ND. The nanoroughness of the NDs in the lowest concentration (0.075% w/v) could be higher than that of SLM-Ti and the other coated substrata. Usually, higher surface roughness correlated to an extensive level of *S. aureus* density.[48,69] Further investigation is required to determine the exact mechanism for such antifouling nature of the substrata.

4. CONCLUSIONS

In this study, we have demonstrated that coatings containing NDs could be applied on 3D-printed SLM-Ti substrata. The surface coverage of ND could be controlled by adjusting the ND concentration, and in this study, suspensions of concentrations 0.075, 0.75, and 7.5% w/v were used to apply the surface coatings. This study utilized a dip-coating method to create coatings that were simple, fast, and cost effective, and the resulting surfaces were shown to improve the biocompatibility of 3D-printed SLM-Ti substrata. The addition of an ND coating to the SLM-Ti substrata resulted in the formation of a surface that directly affected the HDF cell growth and *S. aureus* colonization on these samples in a surface coverage-dependent manner. After 3 days of incubation, the greatest HDF and OB cell densities were found on the samples coated with the highest concentration of ND (7.5% w/v). The same high concentration of ND-coated substrata also resulted in the lowest amount of *S. aureus* adhesion and growth compared with that obtained on the uncoated SLM-Ti substrata. As 3D-printed SLM-Ti finds more applications in the formation of orthopedic implants, modifying their surface with ND may provide a preferable cell−implant interface compared with that exhibited by traditional SLM-Ti implants. The results of this study indicated that ND-coated SLM-Ti may be suitable for both internal fixation devices and subcutaneous implants. ND-coated SLM-Ti implants could prolong the lifetime of these devices, ultimately improving patient outcomes.

■ ASSOCIATED CONTENT

Supporting Information

The Supporting Information is available free of charge on the ACS Publications website at DOI: 10.1021/acsami.9b07064.

Brief video showing the attachment of human dermal fibroblast cells on nanodiamond (7.5% w/v)-coated selective laser melted titanium (Video S1) (ZIP)

■ AUTHOR INFORMATION

Corresponding Authors

*E-mail: s3382184@student.rmit.edu.au (A.R.).
*E-mail: kate.fox@rmit.edu.au (K.F.).

ORCID

Aaqil Rifai: 0000-0002-3736-943X
Nhiem Tran: 0000-0002-0209-2434
Aaron Elbourne: 0000-0002-4472-4372
Edwin Mayes: 0000-0001-6668-444X
Avik Sarker: 0000-0001-8385-4164
Elena P. Ivanova: 0000-0002-5509-8071
Takeshi Ohshima: 0000-0002-7850-3164
Brant C. Gibson: 0000-0002-7109-2796
Andrew D. Greentree: 0000-0002-3505-9163
Kate Fox: 0000-0001-8090-3215

Funding

K.F. is supported by the Clive and Vera Ramaciotti Foundation and the CASS Foundation (Medicine and Science). K.F. also acknowledges the Australian Research Council (ARC) for funding (IC160100026). B.C.G. and A.D.G. acknowledge the Australian Research Council (ARC) for the funding (CE140100003 and FT160100357).

Notes

The authors declare no competing financial interest.

■ ACKNOWLEDGMENTS

The authors acknowledge the facilities and technical assistance of the RMIT Advanced Manufacturing Precinct. The authors wish to acknowledge the ARC Centre for Nanoscale Biophotonics for sample preparation. The authors would like to acknowledge that the equipment and facilities in the RMIT MicroNano Research Facility were made available for this research. The authors also appreciate the access granted to the facilities and the scientific and technical assistance of the Australian Microscopy & Microanalysis Research Facility at RMIT University. This work was supported by a CASS Foundation (Medicine and Science) Grant. NT and PR acknowledge funding through the RMIT Vice-Chancellor's Research Fellowships.

■ REFERENCES

(1) Mantripragada, V. P.; Lecka-Czernik, B.; Ebraheim, N. A.; Jayasuriya, A. C. An Overview of Recent Advances in Designing Orthopedic and Craniofacial Implants. *J. Biomed. Mater. Res., Part A* **2013**, *101*, 3349−3364.

(2) Balasundaram, I.; Al-Hadad, I.; Parmar, S. Recent Advances in Reconstructive Oral and Maxillofacial Surgery. *Br. J. Oral Maxillofac. Surg.* **2012**, *50*, 695−705.

(3) Shidid, D.; Leary, M.; Choong, P.; Brandt, M. Just-in-Time Design and Additive Manufacture of Patient-Specific Medical Implants. *Phys. Procedia* **2016**, *83*, 4−14.

(4) Ramezanian, M.; Mahmoud-Hashemi, H.; Vaezi, T.; Beshkar, M.; Hasheminasab, M. The Pattern of Maxillofacial Fractures: A Study of 302 Patients and a Discussion of Fracture Classification. *J. Craniomaxillofac. Res.* **2015**, *1*, 95−102.

(5) Olszewski, R. Three-Dimensional Rapid Prototyping Models in Cranio-Maxillofacial Surgery: Systematic Review and New Clinical Applications. *Proc. Belgian R. Acad. Med.* **2013**, *2*, 43−77.

(6) Zhu, C.; Liu, T.; Qian, F.; Chen, W.; Chandrasekaran, S.; Yao, B.; Song, Y.; Duoss, E. B.; Kuntz, J. D.; Spadaccini, C. M.; Worsley, M. A.; Li, Y. 3d Printed Functional Nanomaterials for Electrochemical Energy Storage. *Nano Today* **2017**, *15*, 107−120.

DOI: 10.1021/acsami.9b07064
ACS Appl. Mater. Interfaces XXXX, XXX, XXX−XXX

(7) Brandt, M. The Role of Lasers in Additive Manufacturing. In *Laser Additive Manufacturing*; Brandt, M., Ed.; Woodhead Publishing, 2017; pp 1−18.
(8) Kruth, J. P.; Froyen, L.; Van Vaerenbergh, J.; Mercelis, P.; Rombouts, M.; Lauwers, B. Selective Laser Melting of Iron-Based Powder. *J. Mater. Process. Technol.* **2004**, *149*, 616−622.
(9) Mullen, L.; Stamp, R. C.; Brooks, W. K.; Jones, E.; Sutcliffe, C. J. Selective Laser Melting: A Regular Unit Cell Approach for the Manufacture of Porous, Titanium, Bone in-Growth Constructs, Suitable for Orthopedic Applications. *J. Biomed. Mater. Res., Part B* **2009**, *89B*, 325−334.
(10) Amstutz, H. C.; Campbell, P.; Kossovsky, N.; Clarke, I. C. Mechanism and Clinical Significance of Wear Debris-Induced Osteolysis. *Clin. Orthop. Relat. Res.* **1992**, *276*, 7−18.
(11) Zhao, L.; Chu, P. K.; Zhang, Y.; Wu, Z. Antibacterial Coatings on Titanium Implants. *J. Biomed. Mater. Res., Part B* **2009**, *91B*, 470−480.
(12) Van Noort, R. Titanium: The Implant Material of Today. *J. Mater. Sci.* **1987**, *22*, 3801−3811.
(13) Rats, D.; Vandenbulcke, L.; Herbin, R.; Benoit, R.; Erre, R.; Serin, V.; Sevely, J. Characterization of Diamond Films Deposited on Titanium and Its Alloys. *Thin Solid Films* **1995**, *270*, 177−183.
(14) Wooley, P. H.; Schwarz, E. M. Aseptic Loosening. *Gene Ther.* **2004**, *11*, 402.
(15) Sundfeldt, M.; Carlsson, L. V.; Johansson, C. B.; Thomsen, P.; Gretzer, C. Aseptic Loosening, Not Only a Question of Wear: A Review of Different Theories. *Acta Orthop.* **2006**, *77*, 177−197.
(16) Landgraeber, S.; Jäger, M.; Jacobs, J. J.; Hallab, N. J. The Pathology of Orthopedic Implant Failure Is Mediated by Innate Immune System Cytokines. *Mediators Inflammation* **2014**, *2014*, No. 185150.
(17) Costerton, J.; Montanaro, L.; Arciola, C. Biofilm in Implant Infections: Its Production and Regulation. *Int. J. Artif. Organs* **2005**, *28*, 1062−1068.
(18) Hall-Stoodley, L.; Costerton, J. W.; Stoodley, P. Bacterial Biofilms: From the Natural Environment to Infectious Diseases. *Nat. Rev. Microbiol.* **2004**, *2*, 95.
(19) Hoenders, C. S.; Harmsen, M. C.; van Luyn, M. J. The Local Inflammatory Environment and Microorganisms in "Aseptic" Loosening of Hip Prostheses. *J. Biomed. Mater. Res., Part B* **2008**, *86*, 291−301.
(20) Greenfield, E. M.; Bechtold, J. What Other Biologic and Mechanical Factors Might Contribute to Osteolysis? *J. Am. Acad. Orthop. Surg.* **2008**, *16*, S56−S62.
(21) Neut, D.; van Horn, J. R.; van Kooten, T. G.; van der Mei, H. C.; Busscher, H. J. Detection of Biomaterial-Associated Infections in Orthopaedic Joint Implants. *Clin. Orthop. Relat. Res.* **2003**, *413*, 261−268.
(22) Rifai, A.; Tran, N.; Lau, D. W.; Elbourne, A.; Zhan, H.; Stacey, A. D.; Mayes, E. L.; Sarker, A.; Ivanova, E. P.; Crawford, R. J.; et al. Polycrystalline Diamond Coating of Additively Manufactured Titanium for Biomedical Applications. *ACS Appl. Mater. Interfaces* **2018**, *10*, 8474−8484.
(23) Biasetto, L.; Elsayed, H.; Bonollo, F.; Colombo, P. Polymer-Derived Sphene Biocoating on Cpti Substrates for Orthopedic and Dental Implants. *Surf. Coat. Technol.* **2016**, 140−147.
(24) Skoog, S. A.; Kumar, G.; Zheng, J.; Sumant, A. V.; Goering, P. L.; Narayan, R. J. Biological Evaluation of Ultrananocrystalline and Nanocrystalline Diamond Coatings. *J. Mater. Sci.: Mater. Med.* **2016**, *27*, 187.
(25) Raphel, J.; Holodniy, M.; Goodman, S. B.; Heilshorn, S. C. Multifunctional Coatings to Simultaneously Promote Osseointegration and Prevent Infection of Orthopaedic Implants. *Biomaterials* **2016**, *84*, 301−314.
(26) Gallo, J.; Holinka, M.; Moucha, C. S. Antibacterial Surface Treatment for Orthopaedic Implants. *Int. J. Mol. Sci.* **2014**, *15*, 13849.
(27) Costerton, J. W.; Stewart, P. S.; Greenberg, E. P. Bacterial Biofilms: A Common Cause of Persistent Infections. *Science* **1999**, *284*, 1318−1322.
(28) Fritz, J. M.; McDonald, J. R. Osteomyelitis: Approach to Diagnosis and Treatment. *Physician Sportsmed.* **2008**, *36*, 50−54.
(29) Uçkay, I.; Assal, M.; Legout, L.; Rohner, P.; Stern, R.; Lew, D.; Hoffmeyer, P.; Bernard, L. Recurrent Osteomyelitis Caused by Infection with Different Bacterial Strains without Obvious Source of Reinfection. *J. Clin. Microbiol.* **2006**, *44*, 1194−1196.
(30) Mochalin, V. N.; Shenderova, O.; Ho, D.; Gogotsi, Y. The Properties and Applications of Nanodiamonds. *Nat. Nanotechnol.* **2012**, *7*, 11−23.
(31) Taylor, A. C.; González, C. H.; Miller, B. S.; Edgington, R. J.; Ferretti, P.; Jackman, R. B. Surface Functionalisation of Nanodiamonds for Human Neural Stem Cell Adhesion and Proliferation. *Sci. Rep.* **2017**, *7*, No. 7307.
(32) Rifai, A.; Pirogova, E.; Fox, K. Diamond, Carbon Nanotubes and Graphene for Biomedical Applications. *Encyclopedia of Biomedical Engineering*; Elsevier, 2014.
(33) Amaral, M.; Dias, A.; Gomes, P.; Lopes, M.; Silva, R.; Santos, J.; Fernandes, M. Nanocrystalline Diamond: In Vitro Biocompatibility Assessment by Mg63 and Human Bone Marrow Cells Cultures. *J. Biomed. Mater. Res., Part A* **2008**, *87A*, 91−99.
(34) Merkel, T. J.; DeSimone, J. M. Dodging Drug-Resistant Cancer with Diamonds. *Sci. Transl. Med.* **2011**, *3*, No. 73ps8.
(35) Wehling, J.; Dringen, R.; Zare, R. N.; Maas, M.; Rezwan, K. Bactericidal Activity of Partially Oxidized Nanodiamonds. *ACS Nano* **2014**, *8*, 6475−6483.
(36) Zhang, Q.; Mochalin, V. N.; Neitzel, I.; Knoke, I. Y.; Han, J.; Klug, C. A.; Zhou, J. G.; Lelkes, P. I.; Gogotsi, Y. Fluorescent PLLA-Nanodiamond Composites for Bone Tissue Engineering. *Biomaterials* **2011**, *32*, 87−94.
(37) Mansoorianfar, M.; Shokrgozar, M. A.; Mehrjoo, M.; Tamjid, E.; Simchi, A. Nanodiamonds for Surface Engineering of Orthopedic Implants: Enhanced Biocompatibility in Human Osteosarcoma Cell Culture. *Diamond Relat. Mater.* **2013**, *40*, 107−114.
(38) Fox, K.; Palamara, J.; Judge, R.; Greentree, A. D. Diamond as a Scaffold for Bone Growth. *J. Mater. Sci.: Mater. Med.* **2013**, *24*, 849−861.
(39) Papo, M. J.; Catledge, S. A.; Vohra, Y. K.; Machado, C. Mechanical Wear Behavior of Nanocrystalline and Multilayer Diamond Coatings on Temporomandibular Joint Implants. *J. Mater. Sci.: Mater. Med.* **2004**, *15*, 773−777.
(40) Amaral, M.; Gomes, P. S.; Lopes, M. A.; Santos, J. D.; Silva, R. F.; Fernandes, M. H. Nanocrystalline Diamond as a Coating for Joint Implants: Cytotoxicity and Biocompatibility Assessment. *J. Nanomater.* **2008**, *2008*, No. 894352.
(41) Catledge, S. A.; Thomas, V.; Vohra, Y. Nanostructured Diamond Coatings for Orthopaedic Applications. *Diamond-Based Materials for Biomedical Applications*; Woodhead Publishing Series in Biomaterials; Woodhead Publishing: 2013; Vol. *2013*, pp 105−150.
(42) Hayward, I.; Singer, I. The Tribological Behaviour of Diamond Coatings. *New Diamond Sci. Technol.* **1991**, 785−789.
(43) Fox, K.; Tran, P. A.; Lau, D. W.; Ohshima, T.; Greentree, A. D.; Gibson, B. C. Nanodiamond-Polycaprolactone Composite: A New Material for Tissue Engineering with Sub-Dermal Imaging Capabilities. *Mater. Lett.* **2016**, *185*, 185−188.
(44) Hasan, J.; Crawford, R. J.; Ivanova, E. P. Antibacterial Surfaces: The Quest for a New Generation of Biomaterials. *Trends Biotechnol.* **2013**, *31*, 295−304.
(45) Quiryen, M.; Listgarten, M. The Distribution of Bacterial Morphotypes around Natural Teeth and Titanium Implants Ad Modum Brånemark. *Clin. Oral Implants Res.* **1990**, *1*, 8−12.
(46) Yoshinari, M.; Oda, Y.; Kato, T.; Okuda, K. Influence of Surface Modifications to Titanium on Antibacterial Activity in Vitro. *Biomaterials* **2001**, *22*, 2043−2048.
(47) Subbiahdoss, G.; Pidhatika, B.; Coullerez, G.; Charnley, M.; Kuijer, R.; van der Mei, H. C.; Textor, M.; Busscher, H. J. Bacterial Biofilm Formation Versus Mammalian Cell Growth on Titanium-Based Mono- and Bi-Functional Coating. *Eur. Cell Mater.* **2010**, *19*, 205−213.

DOI: 10.1021/acsami.9b07064
ACS Appl. Mater. Interfaces XXXX, XXX, XXX−XXX

(48) Ivanova, E. P.; Truong, V. K.; Wang, J. Y.; Berndt, C. C.; Jones, R. T.; Yusuf, I. I.; Peake, I.; Schmidt, H. W.; Fluke, C.; Barnes, D.; Crawford, R. J. Impact of Nanoscale Roughness of Titanium Thin Film Surfaces on Bacterial Retention. *Langmuir* **2010**, *26*, 1973−1982.
(49) Braem, A.; Van Mellaert, L.; Mattheys, T.; Hofmans, D.; De Waelheyns, E.; Geris, L.; Anné, J.; Schrooten, J.; Vleugels, J. Staphylococcal Biofilm Growth on Smooth and Porous Titanium Coatings for Biomedical Applications. *J. Biomed. Mater. Res., Part A* **2014**, *102*, 215−224.
(50) Xu, J.-y.; Chen, X.-s.; Zhang, C.-y.; Liu, Y.; Wang, J.; Deng, F.-l. Improved Bioactivity of Selective Laser Melting Titanium: Surface Modification with Micro-/Nano-Textured Hierarchical Topography and Bone Regeneration Performance Evaluation. *Mater. Sci. Eng., C* **2016**, *68*, 229−240.
(51) Lim, T.-S.; Fu, C.-C.; Lee, K.-C.; Lee, H.-Y.; Chen, K.; Cheng, W.-F.; Pai, W. W.; Chang, H.-C.; Fann, W. Fluorescence Enhancement and Lifetime Modification of Single Nanodiamonds near a Nanocrystalline Silver Surface. *Phys. Chem. Chem. Phys.* **2009**, *11*, 1508−1514.
(52) Behler, K. D.; Stravato, A.; Mochalin, V.; Korneva, G.; Yushin, G.; Gogotsi, Y. Nanodiamond-Polymer Composite Fibers and Coatings. *ACS Nano* **2009**, *3*, 363−369.
(53) Heffernan, A. H.; Greentree, A. D.; Gibson, B. C. Nanodiamond Arrays on Glass for Quantification and Fluorescence Characterisation. *Sci. Rep.* **2017**, *7*, No. 9252.
(54) ASTM Designation: D 3359-97 Standard Test Methods for Measuring Adhesion by Tape Test.
(55) Isackson, D.; McGill, L. D.; Bachus, K. N. Percutaneous Implants with Porous Titanium Dermal Barriers: An in Vivo Evaluation of Infection Risk. *Med. Eng. Phys.* **2011**, *33*, 418−426.
(56) Yang, L.; Sheldon, B. W.; Webster, T. J. The Impact of Diamond Nanocrystallinity on Osteoblast Functions. *Biomaterials* **2009**, *30*, 3458−3465.
(57) Sarker, A.; Tran, N.; Rifai, A.; Elambasseril, J.; Brandt, M.; Williams, R.; Leary, M.; Fox, K. Angle Defines Attachment: Switching the Biological Response to Titanium Interfaces by Modifying the Inclination Angle During Selective Laser Melting. *Mater. Des.* **2018**, *154*, 326−339.
(58) Arnault, J. Surface Modifications of Nanodiamonds and Current Issues for Their Biomedical Applications. *Novel Aspects of Diamond*; Springer, 2015; pp 85−122.
(59) Schrand, A. M.; Hens, S. A. C.; Shenderova, O. A. Nanodiamond Particles: Properties and Perspectives for Bioapplications. *Crit. Rev. Solid State Mater. Sci.* **2009**, *34*, 18−74.
(60) Zhao, F.; Vrajitoarea, A.; Jiang, Q.; Han, X.; Chaudhary, A.; Welch, J. O.; Jackman, R. B. Graphene-Nanodiamond Heterostructures and Their Application to High Current Devices. *Sci. Rep.* **2015**, *5*, No. 13771.
(61) Schneider, C. A.; Rasband, W. S.; Eliceiri, K. W. Nih Image to Imagej: 25 Years of Image Analysis. *Nat. Methods* **2012**, *9*, 671.
(62) Gittens, R. A.; Scheideler, L.; Rupp, F.; Hyzy, S. L.; Geis-Gerstorfer, J.; Schwartz, Z.; Boyan, B. D. A Review on the Wettability of Dental Implant Surfaces Ii: Biological and Clinical Aspects. *Acta Biomater.* **2014**, *10*, 2907−2918.
(63) Lampin, M.; Warocquier-Clérout, R.; Legris, C.; Degrange, M.; Sigot-Luizard, M. Correlation between Substratum Roughness and Wettability, Cell Adhesion, and Cell Migration. *J. Biomed. Mater. Res., Part A* **1997**, *36*, 99−108.
(64) Altankov, G.; Groth, T. Reorganization of Substratum-Bound Fibronectin on Hydrophilic and Hydrophobic Materials Is Related to Biocompatibility. *J. Mater. Sci.: Mater. Med.* **1994**, *5*, 732−737.
(65) Ruardy, T. G.; Schakenraad, J. M.; van der Mei, H. C.; Busscher, H. J. Adhesion and Spreading of Human Skin Fibroblasts on Physicochemically Characterized Gradient Surfaces. *J. Biomed. Mater. Res.* **1995**, *29*, 1415−1423.
(66) Schrand, A. M.; Johnson, J.; Dai, L.; Hussain, S. M.; Schlager, J. J.; Zhu, L.; Hong, Y.; Ōsawa, E. Cytotoxicity and Genotoxicity of Carbon Nanomaterials. *Safety of Nanoparticles*; Springer, 2009; pp 159−187.
(67) Webster, T. J. *Safety of Nanoparticles*; Springer, 2008.
(68) Zhang, W.; Patel, K.; Schexnider, A.; Banu, S.; Radadia, A. D. Nanostructuring of Biosensing Electrodes with Nanodiamonds for Antibody Immobilization. *ACS Nano* **2014**, *8*, 1419−1428.
(69) Elbourne, A.; Coyle, V. E.; Truong, V. K.; Sabri, Y. M.; Kandjani, A. E.; Bhargava, S. K.; Ivanova, E. P.; Crawford, R. J. Multi-Directional Electrodeposited Gold Nanospikes for Antibacterial Surface Applications. *Nanoscale Adv.* **2019**, *1*, 203−212.
(70) Feng, G.; Cheng, Y.; Wang, S.-Y.; Borca-Tasciuc, D. A.; Worobo, R. W.; Moraru, C. I. Bacterial Attachment and Biofilm Formation on Surfaces Are Reduced by Small-Diameter Nanoscale Pores: How Small Is Small Enough? *npj Biofilms Microbiomes* **2015**, *1*, No. 15022.
(71) Chatterjee, A.; Perevedentseva, E.; Jani, M.; Cheng, C.-Y.; Ye, Y.-S.; Chung, P.-H.; Cheng, C.-L. Antibacterial Effect of Ultrafine Nanodiamond against Gram-Negative Bacteria *Escherichia coli*. *J. Biomed. Opt.* **2014**, *20*, No. 051014.
(72) Beranová, J.; Seydlová, G.; Kozak, H.; Potocký, Š.; Konopásek, I.; Kromka, A. Antibacterial Behavior of Diamond Nanoparticles against *Escherichia coli*. *Phys. Status Solidi B* **2012**, *249*, 2581−2584.
(73) Turcheniuk, V.; Raks, V.; Issa, R.; Cooper, I. R.; Cragg, P. J.; Jijie, R.; Dumitrascu, N.; Mikhalovska, L. I.; Barras, A.; Zaitsev, V.; Boukherroub, R.; Szunerits, S. Antimicrobial Activity of Menthol Modified Nanodiamond Particles. *Diamond Relat. Mater.* **2015**, *57*, 2−8.
(74) Coraça-Huber, D. C.; Fille, M.; Hausdorfer, J.; Pfaller, K.; Nogler, M. *Staphylococcus aureus* Biofilm Formation and Antibiotic Susceptibility Tests on Polystyrene and Metal Surfaces. *J. Appl. Microbiol.* **2012**, *112*, 1235−1243.

DOI: 10.1021/acsami.9b07064
ACS Appl. Mater. Interfaces XXXX, XXX, XXX−XXX